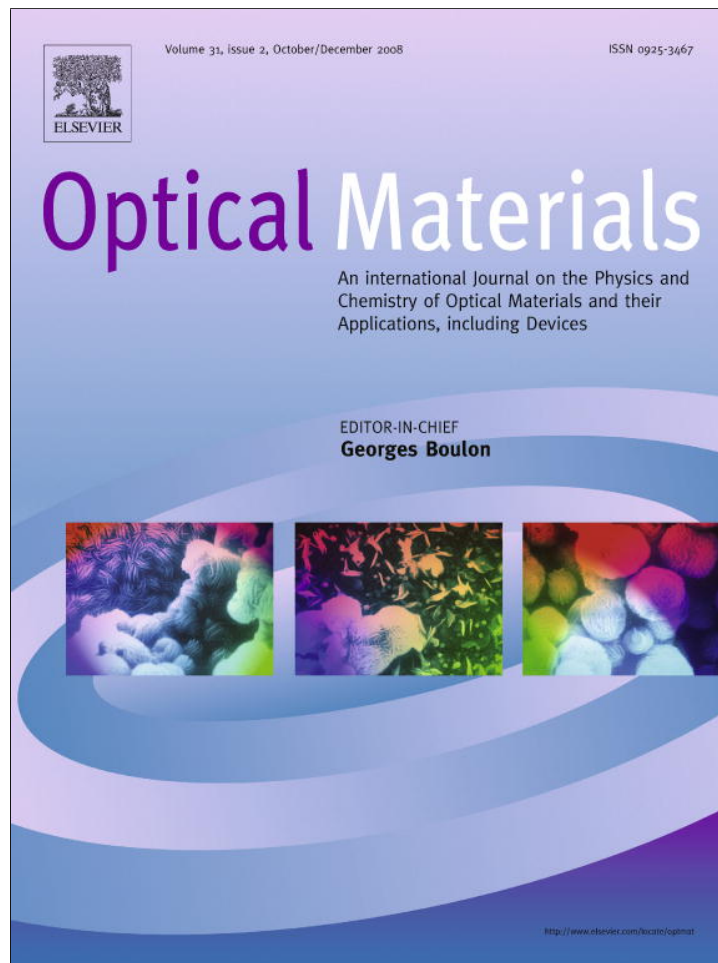


Provided for non-commercial research and education use.
Not for reproduction, distribution or commercial use.



This article appeared in a journal published by Elsevier. The attached copy is furnished to the author for internal non-commercial research and education use, including for instruction at the authors institution and sharing with colleagues.

Other uses, including reproduction and distribution, or selling or licensing copies, or posting to personal, institutional or third party websites are prohibited.

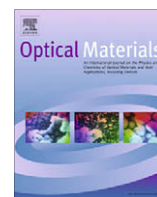
In most cases authors are permitted to post their version of the article (e.g. in Word or Tex form) to their personal website or institutional repository. Authors requiring further information regarding Elsevier's archiving and manuscript policies are encouraged to visit:

<http://www.elsevier.com/copyright>



Contents lists available at ScienceDirect

Optical Materials

journal homepage: www.elsevier.com/locate/optmatYb³⁺ quenching effects in co-doped polycrystalline BaTiO₃:Er³⁺, Yb³⁺M.A. Meneses-Nava^{a,*}, O. Barbosa-García^a, J.L. Maldonado^a, G. Ramos-Ortíz^a, J.L. Pichardo^a, M. Torres-Cisneros^b, M. García-Hernández^c, A. García-Murillo^c, F.J. Carrillo-Romo^c^aCentro de Investigaciones en Óptica, Apdo. Postal 1-948, 37000 León, Guanajuato, Mexico^bFIMEE, Universidad de Guanajuato, Salamanca, Guanajuato, 36730, Mexico^cCentro de Investigación en Ciencia Aplicada y Tecnología Avanzada (CICATA) Unidad Altamira – IPN; Km. 14.5 Carr., Tampico-Puerto Industrial, 89600 Altamira, Tamaulipas, Mexico

ARTICLE INFO

Article history:

Received 4 March 2008

Received in revised form 4 April 2008

Accepted 9 April 2008

Available online 5 June 2008

PACS:

78.55.-m

81.20.Fw

87.64.Ni

Keywords:

Fluorescence

Energy transfer

Spectroscopy

Sol-gel

ABSTRACT

Luminescent properties of single and co-doped samples of sol-gel polycrystalline BaTiO₃ with trivalent Er³⁺ and Yb³⁺ ions are reported. Under 520 nm pumping, visible radiative emission from ²H_{7/2}, ⁴S_{3/2} → ⁴I_{15/2}, and ⁴F_{9/2} → ⁴I_{15/2}; and near infrared emission from ⁴S_{3/2} → ⁴I_{13/2}, ⁴I_{11/2} → ⁴I_{15/2} and ⁴I_{13/2} → ⁴I_{15/2} of Er³⁺ and from ²F_{5/2} → ²F_{7/2} of Yb³⁺ ions were measured. For single Er³⁺ doped samples, concentration quenching was observed from the ⁴S_{3/2} state, whereas emissions in the 1.0 and 1.5 μm regions increase with concentration due to the cross-relaxation mechanism ⁴S_{3/2} + ⁴I_{15/2} → ⁴I_{9/2} + ⁴I_{13/2}. Upon addition of Yb³⁺ ions quenching is enhanced, as corroborated by the luminescence decay time curves and emission spectra. This is so because an additional non-radiative energy transfer process from the thermally coupled states (²H_{11/2}, ⁴S_{3/2}) of Er³⁺ to the ²F_{7/2} state of Yb³⁺ takes place.

© 2008 Elsevier B.V. All rights reserved.

1. Introduction

The study of luminescence properties of rare earth elements hosted in new matrices, such as polycrystalline and nano-structured materials is very important [1–3]. In particular, besides that Barium Titanate (BaTiO₃) is an interesting example of ferro-electric material [4–8], it has been studied regarding its luminescent properties when doped with rare earth elements, such as Er³⁺ and Eu³⁺ [9,10]. Its perovskite structure allows hosting ions of different size and a large quantity of doping can be accommodated without major difficulties [11,12]. Further, different sol-gel routes have been reported in addition to the traditional mono-crystal methods to obtain high quality matrices [13–16]. One major advantage in using the sol-gel technique is to obtain pure nano-scaled powders in a low temperature procedure. Therefore by using the sol-gel technique and properties of the perovskite structure one could dope the BaTiO₃ with rare earth elements and study the luminescence properties. In particular, when a matrix is doped with trivalent Er³⁺ green, red and infrared emissions at about 1.0 and 1.5 μm are obtained. However, when doped together with Yb³⁺ ions some

new mechanisms are reported and the intensity of those emissions changes significantly. Such is the case for those ions in Y₃Al₅O₁₂ and Y₂O₃ nanocrystals [17,18], where the red band emission from Er³⁺ increases its intensity when Yb³⁺ ions are added. The nature of luminescent properties of new materials doped with rare earth elements are based on non-radiative energy transfer, cross-relaxation and up-conversion mechanisms, to name some of them. Further, one mechanism might overcome to another depending on the doping concentration, nature of the matrix (mono-crystal or polycrystal obtained through a sol-gel method) and the pumping wavelength. In this work we have sensitized BaTiO₃ through the sol-gel method with single and co-doped Er³⁺ and Yb³⁺ ions. All samples were studied for luminescent properties and pumped at 520 nm wavelength.

2. Experimental

BaTiO₃ samples were synthesized through the sol-gel method and thermally treated at 700 °C in air for 8 h. Sample composition and concentrations are as follows, four samples are single doped with Er³⁺ at 0.1, 2.5, 5.0 and 10.0 mol%, respectively, and three co-doped samples with Yb³⁺ at fixed concentration of 6.0 mol%

* Corresponding author. Tel.: +52 477 4414200, fax: +52 477 4414209.
E-mail address: tono@cio.mx (M.A. Meneses-Nava).

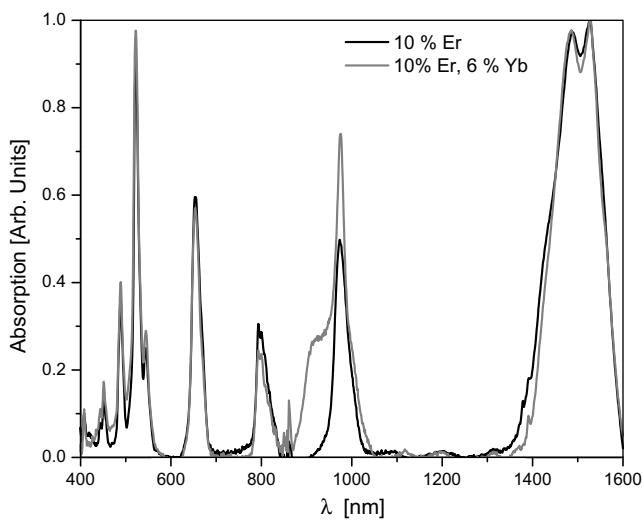


Fig. 1. Absorption spectra of single and co-doped BTO samples at (10%) Er³⁺ and (10%) Er³⁺, (6%) Yb³⁺.

and Er³⁺ at 2.5, 5.0 and 10.0 mol%. For absorption spectra we use a Perkin–Elmer lambda-900 spectrophotometer with a diffuse reflectance integrating sphere. It is important to note that due to sample polycrystalline nature and use of an integrating sphere, absorption spectra only show bands where ions absorb light, but it is not possible to quantify optical density. Luminescence spectra were obtained by pumping samples with a Spectra Physics Quanta-Ray Nd:YAG-MOPO tunable laser system and luminescence collected at right angle by an optical system and dispersed by an Acton Research SpectraPro 500i spectrometer with two Hamamatsu PMT detectors, R555 and R326 for the visible and NIR regions, respectively. Signals from PMT detectors were connected to a Stanford Research SR830 lock-in amplifier controlled by a personal computer. To correct for any laser variation, pumping energy was monitored through a pyroelectric energy meter from Molectron and signal fed into the control computer to do proper corrections. Also care was taken to set samples in the same position by means of a sample holder mounted in a xyz stage and locked in position to be confident in emission intensity comparison for all samples. All measurements were performed at room temperature.

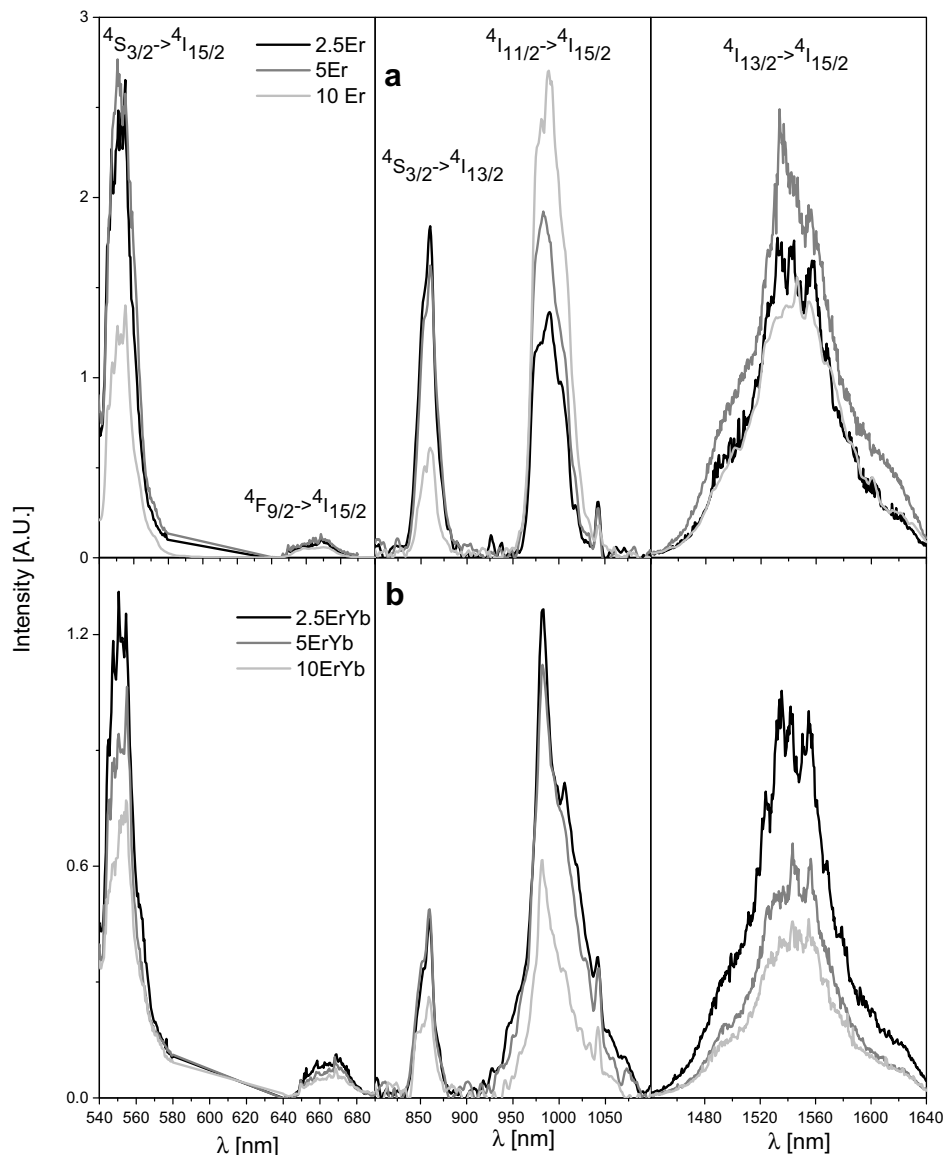


Fig. 2. Fluorescence spectra of single and co-doped BTO samples excited at 520 nm. (a) Single doped Er³⁺:BTO samples, (b) co-doped Er³⁺, Yb³⁺:BTO samples.

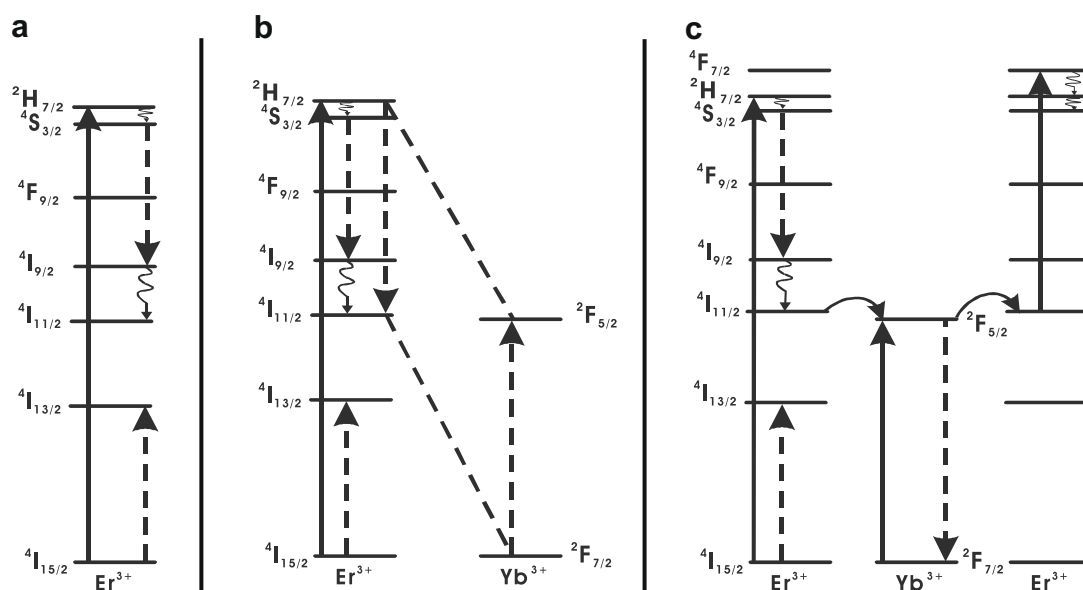


Fig. 3. Energy level diagram showing the most relevant transitions after 520 nm excitation. (a) Schematic of cross-relaxation mechanisms involved to explain the quenching of the ($^2H_{7/2}, ^4S_{3/2}$) \rightarrow $^4I_{15/2}$ transition. (b) Schematic of the non-resonant energy transfer between Er^{3+} and Yb^{3+} ions. (c) Schematic of resonant energy transfer and back transfer between Er^{3+} and Yb^{3+} ions.

3. Results and discussion

3.1. Absorption spectra

Single doped samples showed the characteristic bands associated with trivalent Erbium spectrum in the 450–1600 nm region, while co-doped samples showed the same Er^{3+} absorption bands, but the band at about 1.0 μm is modified by the presence of Yb^{3+} ions, as expected, Fig. 1 shows the absorption spectra for samples with 10.0 mol% of Er^{3+} and 6.0 mol% of Yb^{3+} . That is, in this region the band was broadened due to the addition of those ions. According to the absorption spectrum, we pumped our samples at two wavelengths, 520 nm and 940 nm, to study fluorescence emissions and the mechanisms involved.

3.2. Fluorescence emission

Single and co-doped samples pumped at 520 nm show green emission and are ascribed to $^2H_{11/2}, ^4S_{3/2} \rightarrow ^4I_{15/2}$ transition. Nevertheless, for single doped samples there is no change in intensity in these green bands when Er^{3+} concentration was increased from 2.5 mol% to 5.0 mol% and a reduction of half the emission at 10 mol% (see Fig. 2a). This concentration quenching can be explained in terms of the cross-relaxation mechanism [9,19–21] $^4S_{3/2} + ^4I_{15/2} \rightarrow ^4I_{9/2} + ^4I_{13/2}$, Fig. 3a. Because cross-relaxation depends on Er^{3+} concentration, the $^4I_{9/2}$ and $^4I_{13/2}$ levels get more populated at higher concentration. Since no radiative emission from the $^4I_{9/2}$ is observed, a non-radiative transition to the next lower level takes place and from there it relaxes radiatively to the ground level at about 980 nm, i.e. $^4I_{11/2} \rightarrow ^4I_{15/2}$ transition. Therefore, as Er^{3+} concentration increases this transition is stronger and luminescence is more intense as shown in Fig. 2a. Similar behaviour is observed for $^4I_{13/2} \rightarrow ^4I_{15/2}$ transition at about 1.5 μm , Fig. 2a, when Er^{3+} concentration increases from 2.5 to 5.0 mol%, but a quenching at higher concentration is observed, where additional mechanism to depopulate level $^4I_{13/2}$ should be present. Also Fig. 2 shows that there is no emission at 800 nm from $^4I_{9/2}$ level, but an intense luminescence recorded at 860 nm, for all samples. This emission can be ascribed to $^4S_{3/2} \rightarrow ^4I_{13/2}$ transition [22], and is also

quenched with Er^{3+} concentration. This is expected because $^4S_{3/2}$ level depopulates by the above mentioned cross-relaxation mechanism.

Since Er^{3+} concentration is high enough, 2.5, 5.0 and 10.0 mol%, one may consider that additional processes to the assumed cross-relaxation mechanism could be taking place. That is, one may expect to have enough Er^{3+} ions at the $^4I_{11/2}$ level such that a direct energy transfer between two neighbouring excited ions occurs and one of them be promoted to the $^4F_{7/2}$ level and, from there relaxes non-radiatively to the $^2H_{7/2}$ and $^4S_{3/2}$ levels. But this energy transfer up-conversion process should be weak since quenching of green and 860 nm emissions predominates as Er^{3+} concentration increases. A similar process could be expected for two neighbouring Er^{3+} ions at $^4I_{13/2}$ level. For this case one ion transfers its energy to the other and then promoted to the $^4I_{9/2}$ level. Again, we cannot rule out this additional process but its effect should be only present at higher concentrations, as shown in Fig. 2a, where emission in the 1500 nm region is quenched for the 10.0 mol% sample.

It is well known that there is a strong non-radiative energy transfer between Er^{3+} and Yb^{3+} ions due to the overlap of the corresponding absorption and emission spectra [17,23–25]. When co-doped samples were pumped at 520 nm, the $^4I_{11/2}$ level gets populated through the assumed cross-relaxation for single doped samples. It is from this energy level that the non-radiative energy transfer occurs; populating the $^2F_{5/2}$ level of Yb^{3+} (see Fig. 3b). In this case the energy transfer is corroborated by the emission spectra, where a slight broadening of the 1.0 μm emission from the co-doped samples is observed, when compared to single doped samples, Fig. 4, due to the $^2F_{5/2} \rightarrow ^2F_{7/2}$ transition. Further, as the Er^{3+} concentration increases in co-doped samples, the $^4S_{3/2} \rightarrow ^4I_{15/2}$ and the $^4S_{3/2} \rightarrow ^4I_{13/2}$ transitions are quenched as shown in Fig. 2b, and is observed that the emission of these two transitions are smaller when compared with the respective single doped samples, Fig. 4. This extra quenching for co-doped samples can be explained in terms of another non-radiative energy transfer from Er^{3+} to Yb^{3+} ions in close vicinity. In this case an Er^{3+} ion transfers its energy from the thermally coupled levels $^2H_{7/2}$ and $^4S_{3/2}$ to the $^2F_{7/2}$ level of Yb^{3+} , through the $(^2H_{7/2}, ^4S_{3/2}) + ^2F_{7/2} \rightarrow ^4I_{11/2} + ^2F_{5/2}$ transition, as shown in Fig. 3b. Therefore, as

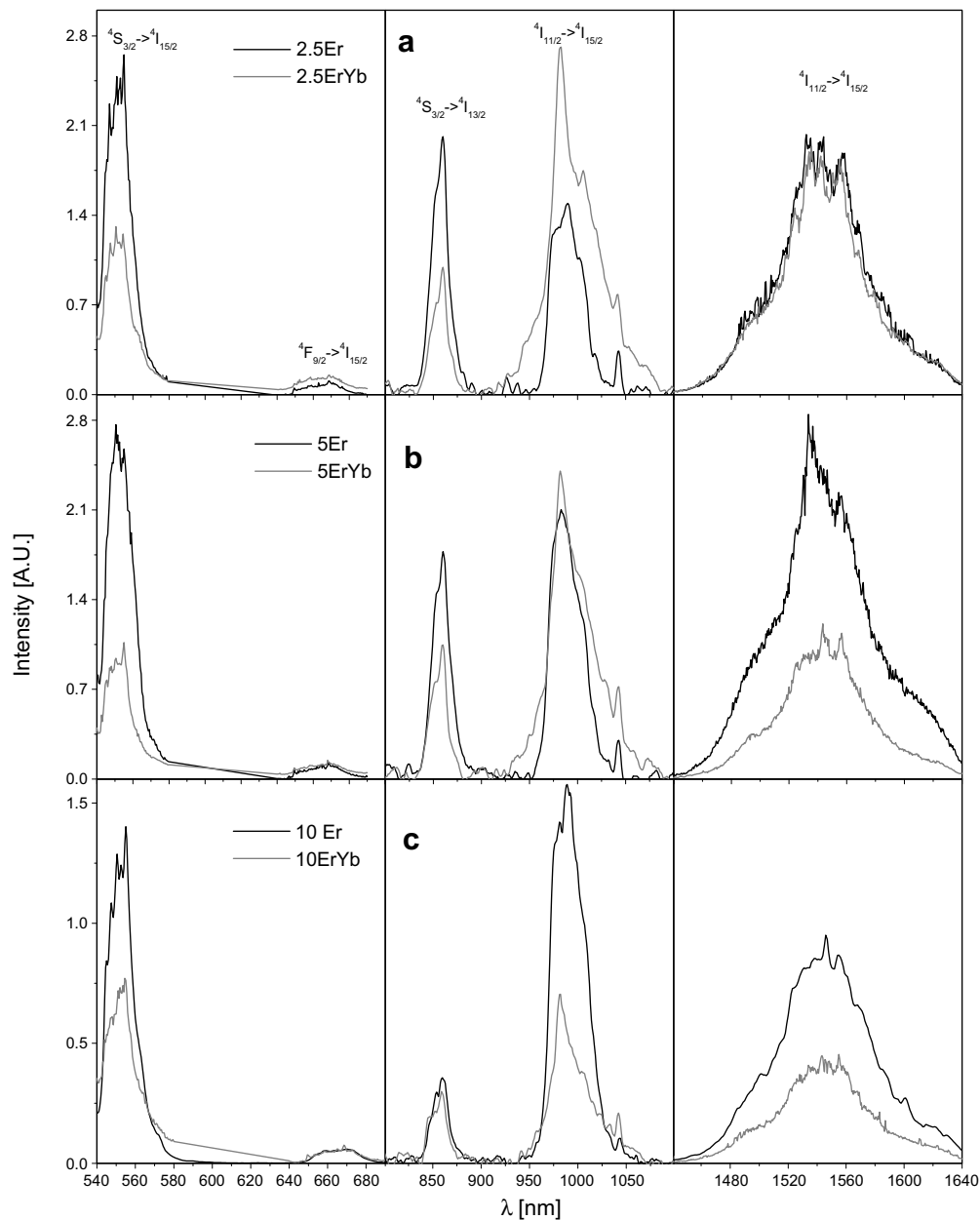


Fig. 4. Effect on Er³⁺ fluorescence spectra after addition of 6% Yb³⁺ ions, excited at 520 nm. (a) 2.5% Er³⁺, (b) 5% Er³⁺ and (c) 10% Er³⁺.

the Er³⁺ concentration increases the thermally coupled levels of Er³⁺ are depopulated and the non-radiative energy transfer is more efficient; thus emissions at about 550 and 860 nm are quenched.

The presence of Yb³⁺ is also observed on the ⁴I_{11/2} → ⁴I_{15/2} and ⁴I_{13/2} → ⁴I_{15/2} transitions, where the emission decrease with Er³⁺ concentration (see Fig. 2b), whereas single doped samples show the reverse behaviour. This behaviour can be explained based on the previous results for single doped samples and the presence of Yb³⁺ ions. For single doped samples the ⁴I_{13/2} state is mainly populated by the assumed cross-relaxation mechanism through the ⁴I_{15/2} → ⁴I_{13/2} transition and the radiative ⁴S_{3/2} → ⁴I_{13/2} transition. However, for co-doped samples the non-radiative energy transfer, (²H_{7/2}, ⁴S_{3/2}) + ²F_{7/2} → ⁴I_{11/2} + ²F_{5/2}, between Er³⁺ and Yb³⁺ overcomes the Er³⁺ cross-relaxation, leaving less population in the ⁴I_{13/2} level. In a similar manner, the ⁴I_{11/2} → ⁴I_{15/2} radiative transition is quenched by the well known non-radiative energy transfer

Table 1

Fluorescence lifetime decays of Er³⁺ in single and co-doped BTO samples and cross-relaxation and energy transfer rates and efficiencies

| Er (%) | τ ₀ (μs) | τ _f (μs) | W _{ET} (10 ³ s ⁻¹) | W _{CR} (10 ³ s ⁻¹) | η _{ET} | η _{CR} |
|-------------------------------------|---------------------|---------------------|----------------------------------------------------|----------------------------------------------------|-----------------|-----------------|
| ⁴S_{3/2} | | | | | | |
| 2.5 | 66.1 | 53.2 | 3.65 | 8.70 | 0.19 | 0.57 |
| 5.0 | 37.6 | 59.7 | – | 20.18 | – | 0.76 |
| 10 | 18.5 | 40.1 | – | 47.52 | – | 0.88 |
| ⁴I_{11/2} | | | | | | |
| 2.5 | 346.7 | 141.4 | 4.19 | 1.78 | 0.59 | 0.62 |
| 5.0 | 97.2 | 175.9 | – | 9.19 | – | 0.89 |
| 10 | 544.8 | 144.1 | 5.1 | 0.73 | 0.74 | 0.40 |
| ⁴I_{13/2} | | | | | | |
| 2.5 | 1566 | 1489 | 0.03 | 0.46 | 0.05 | 0.72 |
| 5.0 | 1032 | 963 | 0.07 | 0.79 | 0.07 | 0.81 |
| 10 | 1789 | 1010 | 0.43 | 0.38 | 0.43 | 0.67 |

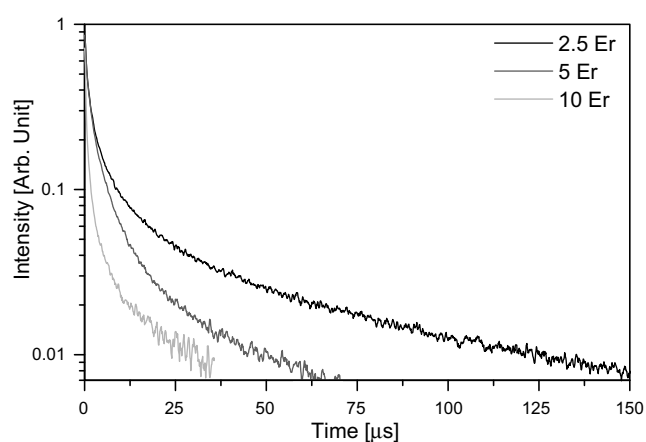


Fig. 5. Fluorescence lifetime decay dependence with Er^{3+} concentration of the $^4\text{S}_{3/2} \rightarrow ^4\text{I}_{15/2}$ transition of single doped samples excited at 520 nm.

between the $^4\text{I}_{11/2}$ level of Er^{3+} to the $^2\text{F}_{5/2}$ level of Yb^{3+} , thus acting the Yb^{3+} ions as quenching centers [17,26], as shown by the emission spectra of Fig. 4.

Besides the green emission band, the red transition $^4\text{F}_{9/2} \rightarrow ^4\text{I}_{15/2}$ was also measured and it is centered at about 665 nm. This emission is affected neither by the Er^{3+} concentration, Fig. 2, nor by the presence of Yb^{3+} ions, Fig. 4, since its peak intensity does not change at all. Thus it was assumed that after pumping at 520 nm, there is a non-radiative transition from the thermally coupled ($^2\text{H}_{7/2}$, $^4\text{S}_{3/2}$) levels to the $^4\text{F}_{9/2}$ level of Er^{3+} . A mechanism to populate the $^4\text{F}_{9/2}$ level, after a 488 nm wavelength pumping has been proposed by Cappobianco et al. [18,27], where a cross-relaxation $^4\text{F}_{7/2} + ^4\text{I}_{11/2} \rightarrow ^4\text{F}_{9/2} + ^4\text{F}_{9/2}$ populate the level, which is concentration dependent. But for that case, however, the green emission does not show quenching and the red emission increases as Er^{3+} concentration increases. After pumping our samples at 488 nm, again no change in intensity of red emission was observed, suggesting that a

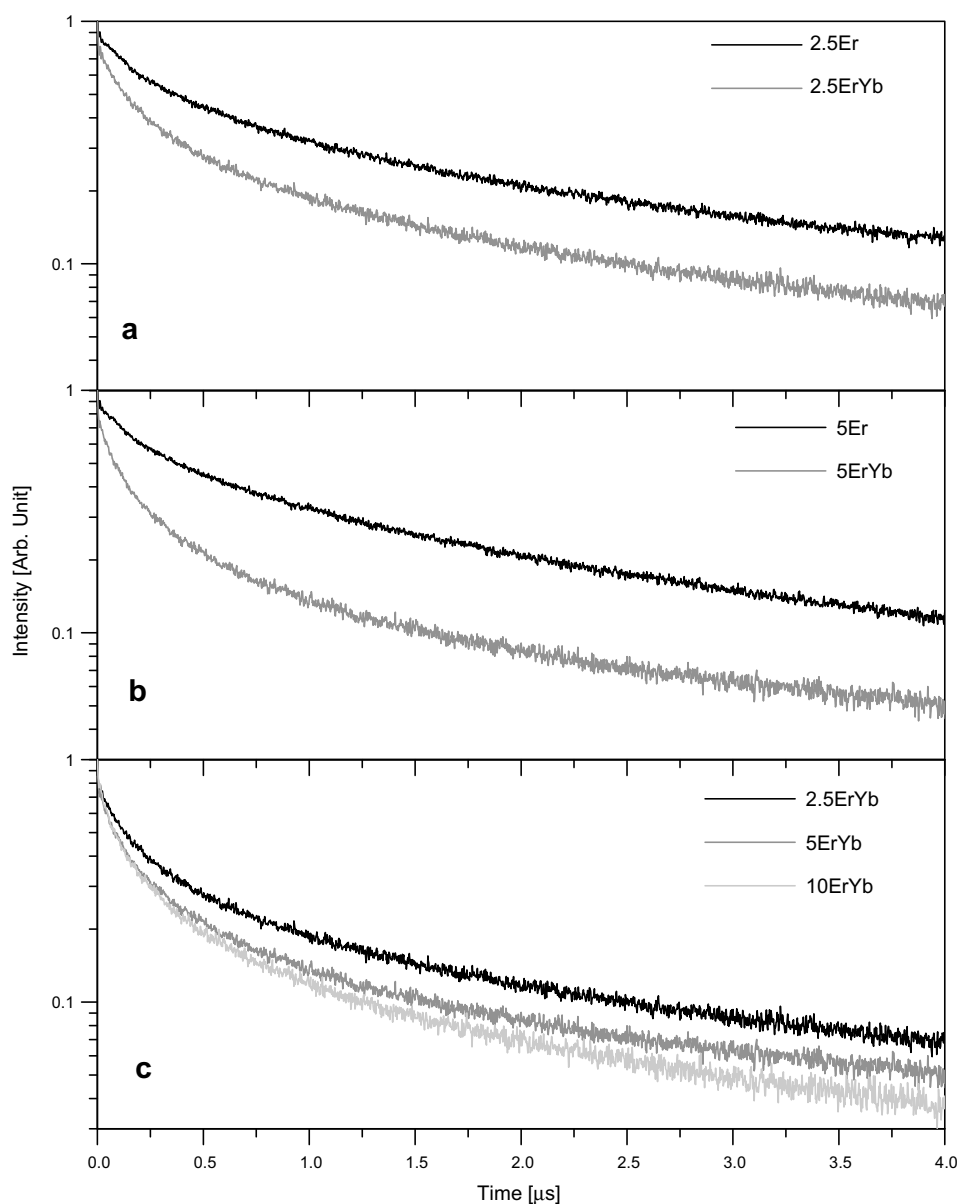


Fig. 6. Effect on Er^{3+} fluorescence lifetime decay of the $^4\text{S}_{3/2} \rightarrow ^4\text{I}_{15/2}$ transition at short times after addition of 6% Yb^{3+} ions excited at 520 nm. (a) 2.5% Er^{3+} , (b) 5% Er^{3+} and (c) Lifetime decay dependence with Er^{3+} concentration.

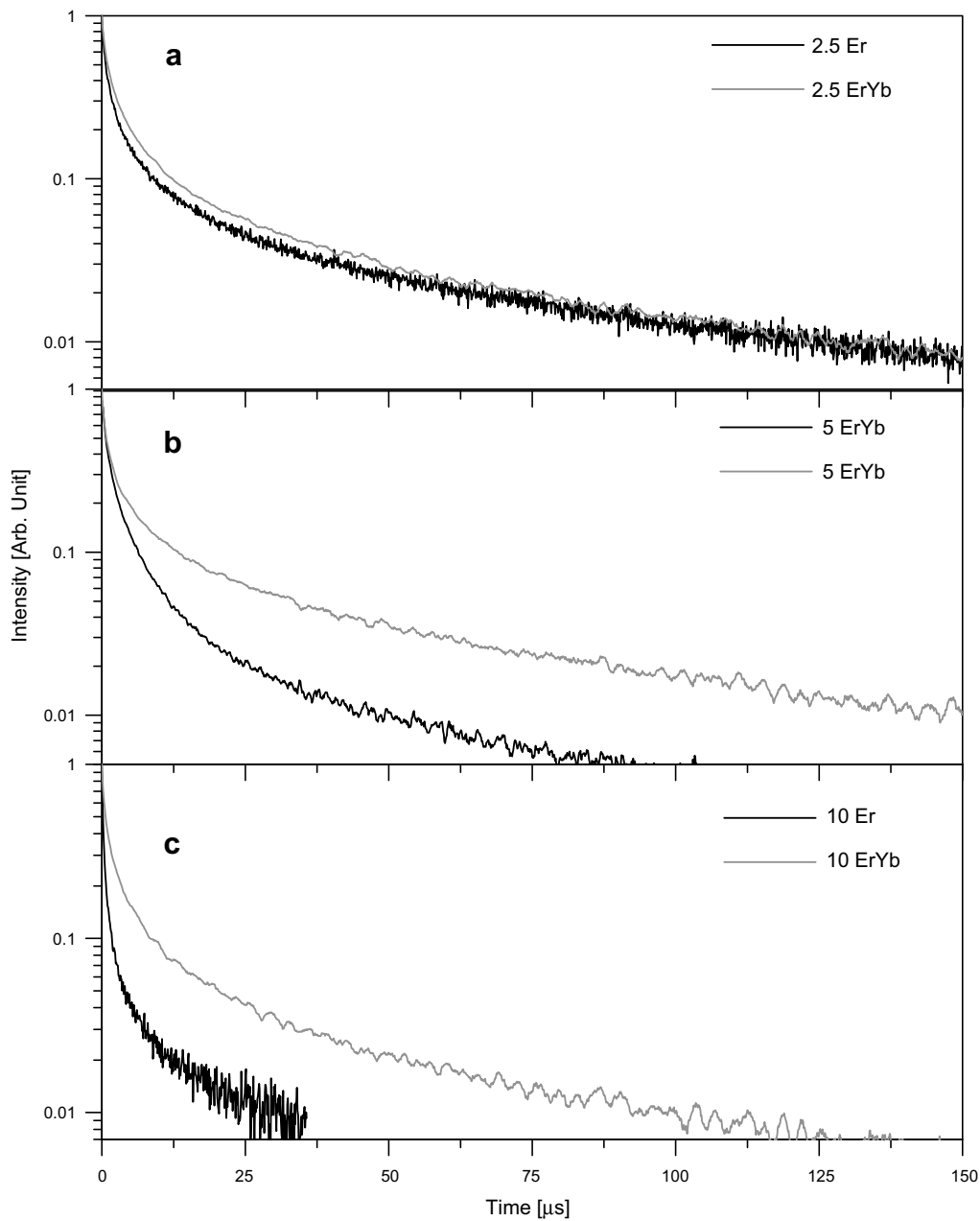


Fig. 7. Effect on Er^{3+} fluorescence lifetime decay of the ${}^4\text{S}_{3/2} \rightarrow {}^4\text{I}_{15/2}$ transition at long times after addition of 6% Yb^{3+} ions excited at 520 nm. (a) 2.5% Er^{3+} , (b) 5% Er^{3+} and (c) 10% Er^{3+} .

non-radiative relaxation from the ${}^4\text{F}_{7/2}$ to the (${}^2\text{H}_{7/2}$, ${}^4\text{S}_{3/2}$) pair levels takes place and from there to the ${}^4\text{F}_{9/2}$ level.

3.3. Lifetime decay

The fluorescence spectra have allowed to establish that a cross-relaxation is responsible for quenching the ${}^4\text{S}_{3/2}$ emission of single doped samples and increasing the emission of ${}^4\text{I}_{11/2}$ and ${}^4\text{I}_{13/2}$ levels as Er^{3+} concentration increases. But the behaviour of those levels is reversed with the presence of Yb^{3+} ions, and it is due to an efficient energy transfer from Er^{3+} to Yb^{3+} . The proposed cross-relaxation and the additional energy transfer mechanism for co-doped samples are further supported by measurements of Er^{3+} lifetime decays of ${}^4\text{S}_{3/2}$, ${}^4\text{I}_{11/2}$ and ${}^4\text{I}_{13/2}$ levels. From these lifetime decays measurements it is possible to estimate some rate values for these two processes from [28]

$$W_{\text{CR}} = \frac{1}{\tau_0} - \frac{1}{\tau_{\text{int}}} \quad (1)$$

$$W_{\text{ET}} = \frac{1}{\tau_f} - \frac{1}{\tau_0} \quad (2)$$

where W_{CR} and W_{ET} are the cross-relaxation and energy transfer rates, respectively; τ_0 is the lifetime decay of single doped samples, τ_{int} is the intrinsic lifetime decay at zero Er^{3+} concentration and τ_f is the lifetime decay of co-doped samples. Decay curves were measured for single and co-doped samples and they are non-exponential, as is expected when energy transfer is present. In this case the lifetime decay was determined through equation [18]:

$$\tau_m = \frac{\int_0^\infty tI(t)dt}{\int_0^\infty I(t)dt} \quad (3)$$

where $I(t)$ is the intensity at time t . The results of lifetime decays and rates are shown in Table 1, together with the respective cross-relaxation and energy transfer efficiencies calculated from equations [28]:

$$\eta_{\text{CR}} = 1 - \frac{\tau_0}{\tau_{\text{int}}} \quad (4)$$

$$\eta_{\text{ET}} = 1 - \frac{\tau_f}{\tau_0} \quad (5)$$

One can observe a reduction with concentration of the lifetime decay of $^4\text{S}_{3/2}$ level for single doped samples, Fig. 5, and the monotonously increase of the cross-relaxation rate and efficiency with concentration, Table 1, thus supporting the proposed cross-relaxation as the quenching mechanism of the green emission.

Addition of Yb^{3+} ions clearly modify the decay trend of the Er^{3+} emission, at early times the lifetime decay for co-doped samples is faster than for single doped samples, Fig. 6a and b, indicating that not only the Er^{3+} cross-relaxation $^4\text{S}_{3/2} + ^4\text{I}_{15/2} \rightarrow ^4\text{I}_{9/2} + ^4\text{I}_{13/2}$ is present, but the additional energy transfer mechanism described above also occurs. This energy transfer is dependent with concentration and a reduction of lifetime decay at higher Er^{3+} concentrations is shown, Fig. 6c. However, at longer times the co-doped samples decay slower than single doped samples, Fig. 7, and the overall decay (τ_f), calculated from Eq. (3) are greater, Table 1. This lengthening of the lifetime decay for co-doped samples can be attributed to an energy back transfer [29,30] from an Yb^{3+} ion in the $^4\text{F}_{5/2}$ to an Er^{3+} ion in the $^4\text{I}_{11/2}$, and from there to the $^4\text{S}_{3/2}$ level, Fig. 3c. Thus the later level is repopulated and consequently

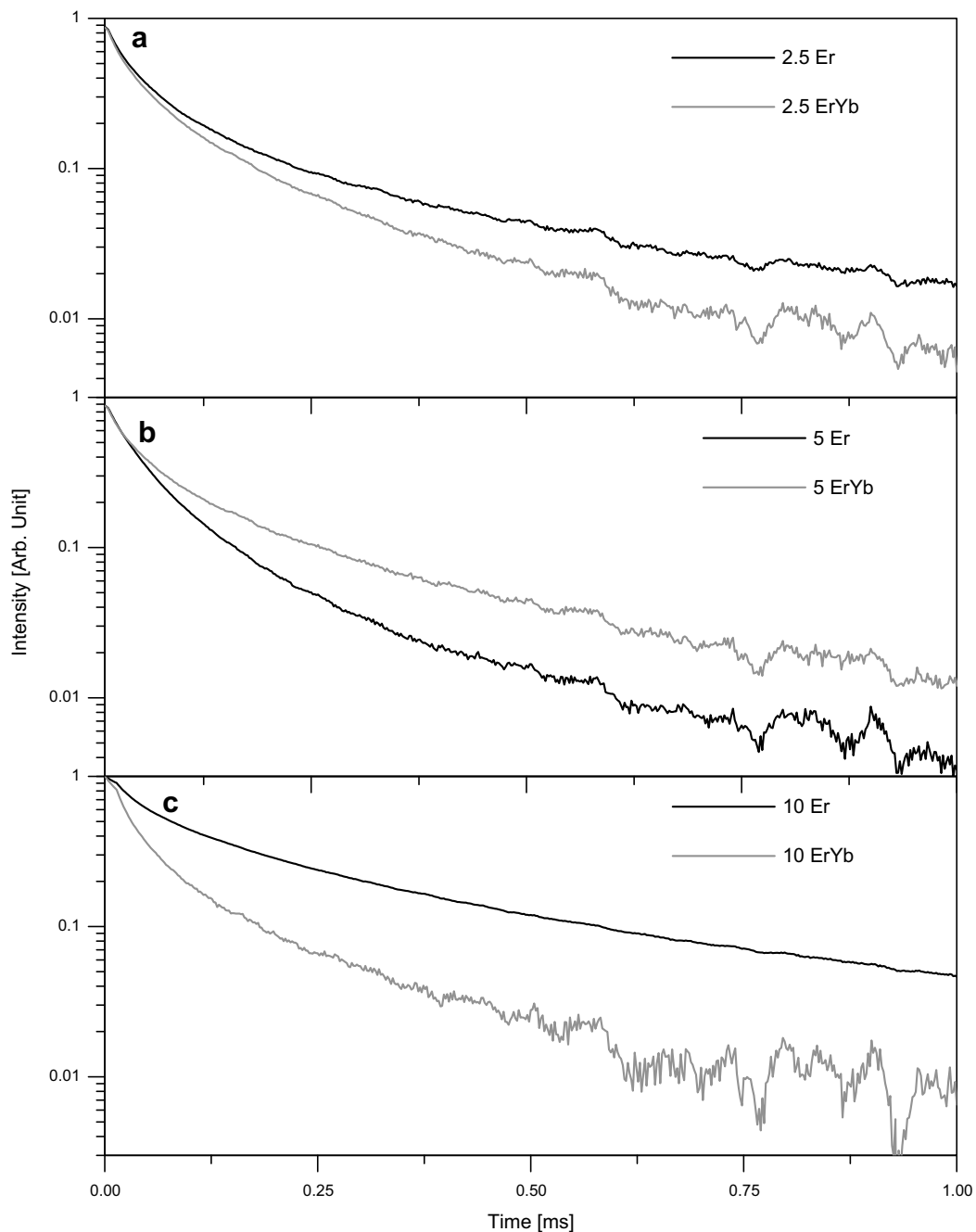


Fig. 8. Effect on Er^{3+} fluorescence lifetime decay of the $^4\text{I}_{11/2} \rightarrow ^4\text{I}_{15/2}$ transition after 6% Yb^{3+} ion addition excited at 520nm. (a) 2.5% Er^{3+} , (b) 5% Er^{3+} and (c) 10% Er^{3+} .

lengthening its lifetime decay. As a result of this process, the $^4I_{11/2}$ level depopulates and its lifetime decay is lower than the corresponding single doped samples, as shown in Fig. 8 and Table 1. The discrepancy of the decay for the 5 mol% sample can be due to the involved competing mechanisms to populate and depopulate level $^4I_{11/2}$, Fig. 3c, since efficiencies for cross-relaxation and energy transfer are similar, Table 1.

Although energy difference between level $^4I_{13/2}$ of Er^{3+} and the $^4F_{5/2}$ of Yb^{3+} is of $3.4 \times 10^3 \text{ cm}^{-1}$, the $^4I_{13/2}$ is influenced by the presence of the Yb^{3+} ions, since lifetime decays of co-doped samples are faster than single doped samples, Fig. 9. But this influence is small since energy transfer rates and efficiency values are smaller than the corresponding values for cross-relaxation, Table 1. So a non-resonant energy transfer from the $^4I_{13/2}$ of Er^{3+} to the $^4F_{5/2}$ of Yb^{3+} , although less probable could be one of the mechanism affecting the $^4I_{13/2}$ luminescence. Another path to depopulate the $^4I_{13/2}$, could be a non-resonant energy back transfer from the $^4F_{5/2}$ level

of Yb^{3+} to the $^4I_{13/2}$ of Er^{3+} , taking it to the $Er^{3+} \ ^4F_{9/2}$ level, but emission of this level does not change significantly for all samples, suggesting that this mechanism is not responsible for quenching the $^4I_{13/2}$ level.

For single doped samples quenching of the green band is explained in terms of a cross-relaxation. Thus it has been shown that due to this cross-relaxation the $^4I_{13/2}$ and $^4I_{11/2}$ levels increase their emissions, while green emission diminishes as Er^{3+} concentration increases. However, when Yb^{3+} ions are present the effect on the emission from those two Er^{3+} levels was reversed; further the Yb^{3+} emission at $1.0 \mu\text{m}$ was also diminished. This quenching of Yb^{3+} luminescence can be explained in terms of the back transfer mechanism discussed above, but when single doped samples with Yb^{3+} ions were excited at 940 nm, emission at 500 nm was measured Fig. 10, suggesting that most probably energy is transferred to Yb^{3+} ions pairs [31,32]. This might be so because Yb^{3+} concentration is high and therefore the distance between two given ions

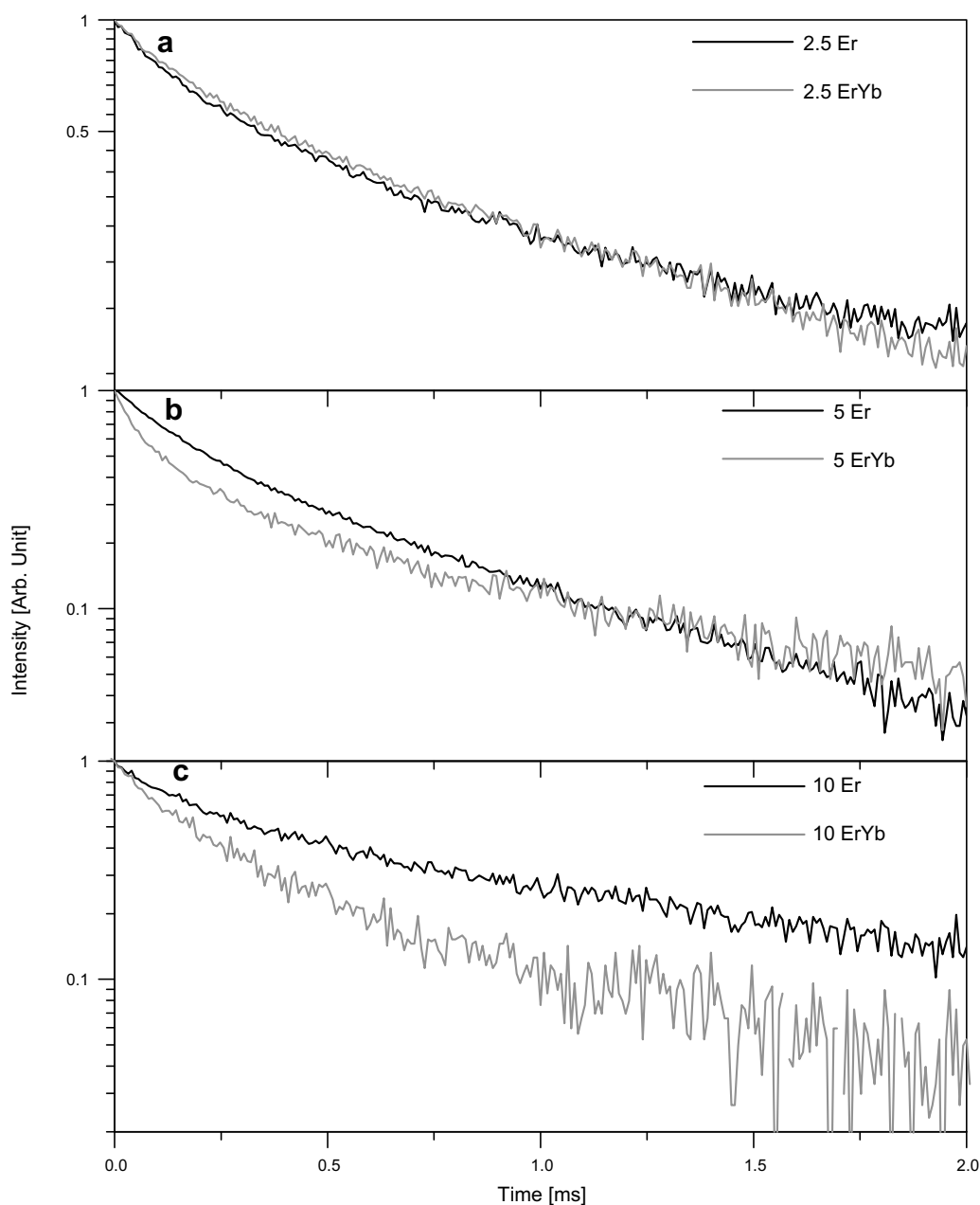


Fig. 9. Effect on Er^{3+} fluorescence lifetime decay of the $^4I_{13/2} \rightarrow ^4I_{15/2}$ transition after 6% Yb^{3+} ion addition excited at 520 nm. (a) 2.5% Er^{3+} , (b) 5% Er^{3+} and (c) 10% Er^{3+}

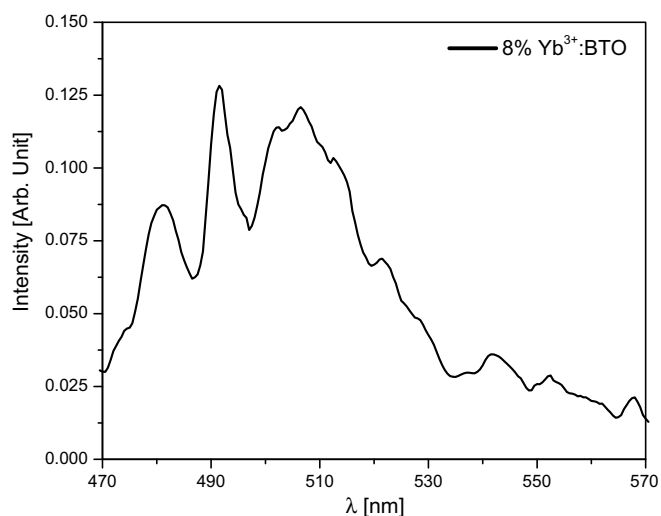


Fig. 10. Yb^{3+} - Yb^{3+} pair emission spectrum of single doped BTO sample at 8% concentration, excited at 915 nm.

should be shorter than at low concentrations. A similar emission was reported by Boulon et al. [33,34], for BaTiO_3 nanocrystals, even at 1.0 mol% Yb^{3+} concentration, therefore the Yb^{3+} ions pairs may act as quenching centers.

4. Conclusion

In this work emission spectra and lifetime decays of single and co-doped Er^{3+} and Yb^{3+} ions in BaTiO_3 polycrystalline sol-gel matrix were measured to describe the mechanisms that drive the fluorescence and the observed quenching. Common to single and co-doped samples was a cross-relaxation mechanism, $^4\text{S}_{3/2} + ^4\text{I}_{15/2} \rightarrow ^4\text{I}_{9/2} + ^4\text{I}_{13/2}$, that quench the green fluorescence and it was shown that this mechanism depends on Er^{3+} concentration. The enhanced concentration quenching in co-doped samples is due to energy transfer between neighbouring Er^{3+} - Yb^{3+} ions. For this case, emission of the $^4\text{I}_{13/2}$ and $^4\text{I}_{11/2}$ levels diminished as Er^{3+} concentration increases; but this behaviour is reversed for single doped Er^{3+} samples. The lengthening of the lifetime decay of $^4\text{S}_{3/2}$ level, in co-doped samples, is due to an energy back transfer, which also affects the quenching of the $^4\text{I}_{11/2}$ level. Further, when single doped Yb^{3+} samples were pumped at 940 nm, an emission from Yb^{3+} pairs was measured at about 500 nm. This process should be present in co-doped Er^{3+} - Yb^{3+} samples and contributes to the quenching of emission at about 1.0 μm .

Acknowledgement

This work was partially supported by CONACYT, Mexico, through Grant SEP-2004-CO1-47805 and CONCYTEG, Gto., through Grant 06-04-k117-88.

References

- [1] T. Kim Anh, L. Quoc Minh, N. Vu, T. Thu Huong, N. Thanh Huong, C. Barthou, W. Streck, *J. Lumin.* 102–103 (2003) 391.
- [2] I.K. Battisha, A. Speghini, S. Polizzi, F. Agnoli, M. Bettinelli, *Mat. Lett.* 57 (2002) 183.
- [3] W. Streck, D. Hreniak, G. Boulon, Y. Guyot, R. Pazzik, *Opt. Mat.* 24 (2003) 15.
- [4] X.X. Liu, L.J. Balk, B.Y. Zhang, Q.R. Yin, *J. Mat. Sci.* 33 (1998) 4543.
- [5] H.J. Hwang, K. Niihara, *J. Mat. Sci.* 33 (1998) 549.
- [6] H. Kishi, N. Kohzu, Y. Iguchi, J. Sugino, M. Kato, H. Ohsato, T. Okuda, *J. Eur. Ceram. Soc.* 21 (2001) 1643.
- [7] B. Li, X. Wang, L. Li, H. Zhou, X. Liu, X. Han, Y. Zhang, X. Qi, X. Deng, *Mat. Chem. Phys.* 83 (2004) 23.
- [8] H. Salehi, S.M. Hosseini, N. Shahtahmasebi, *Ceram. Int.* 30 (2004) 81.
- [9] H.X. Zhang, C.H. Kam, Y. Zhou, X.Q. Han, Q. Xiang, S. Buddhudu, Y.L. Lam, Y.C. Chan, *J. Alloys Compounds* 308 (2000) 134.
- [10] H.X. Zhang, C.H. Kam, Y. Zhou, X.Q. Han, S. Buddhudu, Y.L. Lam, *Opt. Mat.* 15 (2000) 47.
- [11] M.T. Buscaglia, V. Buscaglia, M. Viviani, P. Nanni, M. Hanuskova, *J. Eur. Ceram. Soc.* 20 (2000) 1997.
- [12] Y. Tsur, T.D. Dunbar, C.A. Randall, *J. Electroceram.* 7 (2001) 25.
- [13] H.B. Sharma, A. Mansingh, *J. Mat. Sci.* 33 (1998) 4455.
- [14] H. Kun-Ming, Y. Wein-Duo, H. Chia-Chia, *J. Eur. Ceram. Soc.* 23 (2003) 1901.
- [15] Y. Kobayashi, A. Nishikata, T. Tanase, M. Konno, *J. Sol-Gel Sci. Technol.* 29 (2004) 49.
- [16] O. Harizanov, A. Harizanova, T. Ivanova, *Mat. Sci. Eng. B106* (2004) 191.
- [17] S. Hinojosa, M.A. Meneses-Nava, O. Barbosa-García, L.A. Díaz-Torres, M.A. Santoyo, J.F. Mosiño, *J. Lumin.* 102–103 (2003) 694.
- [18] F. Vetrone, J.C. Boyer, J.A. Capobianco, A. Speghini, M. Bettinelli, *J. Appl. Phys.* 96 (1) (2004) 661.
- [19] C. Duverger, M. Montagna, R. Rolli, S. Ronchin, L. Zampedri, M. Fossi, S. Pelli, G.C. Righini, A. Monteil, C. Armellini, M. Ferrari, *J. Non-Cryst. Solids* 280 (2001) 261.
- [20] J. Castañeda, M.A. Meneses-Nava, O. Barbosa-García, E. De la Rosa-Cruz, J.F. Mosiño, *J. Lumin.* 102–103 (2003) 504.
- [21] J. Castañeda, M.A. Meneses-Nava, O. Barbosa-García, J.L. Maldonado-Rivera, J.F. Mosiño, *Opt. Mat.* 27 (2004) 301.
- [22] S.R. Lüthi, M. Pollnau, H.U. Güdel, M.P. Hehlen, *Phys. Rev. B* 60 (1) (1999) 162.
- [23] S.A. Lopez-Rivera, J. Martín, A. Florez, V. Balassone, *J. Lumin.* 106 (2004) 291.
- [24] S. Bjurshagen, J.E. Hellström, V. Pasiskevicius, M.C. Pujol, M. Aguiló, F. Díaz, *Appl. Opt.* 45 (19) (2006) 4715.
- [25] R. Francini, F. Giovenale, U.M. Grassano, P. Laporta, S. Taccheo, *Opt. Mat.* 13 (2000) 417.
- [26] E.F. Artemev, A.G. Murzin, Y.K. Federov, V.A. Fromzel, *Sov. J. Quantum Electron.* 11 (1981) 1266.
- [27] F. Vetrone, J.C. Boyer, J.A. Capobianco, A. Speghini, M. Bettinelli, *J. Phys. Chem.* 107 (5) (2003) 1107.
- [28] S. Tanabe, K. Suzuki, N. Soga, T. Hanada, *J. Lumin.* 65 (1995) 247.
- [29] J.T. Vega-Duran, O. Barbosa-García, L.A. Díaz-Torres, M.A. Meneses-Nava, D.S. Sumida, *Appl. Phys. Lett.* 76 (2000) 2032.
- [30] B. Simondi-Teisseire, B. Viana, D. Vivien, A.M. Lejus, *Opt. Mat.* 6 (1996) 267.
- [31] X.B. Chen, Y.X. Nie, W.M. Du, N. Sawanobori, *Opt. Comm.* 184 (2000) 289.
- [32] Ph. Goldner, F. Pelle, F. Auzel, *J. Lumin.* 72–74 (1997) 901.
- [33] J. Amami, D. Hreniak, Y. Guyot, R. Pazzik, C. Goutaudier, G. Boulon, M. Ayadi, W. Streck, *J. Lumin.* 119–120 (2006) 383.
- [34] J. Amami, D. Hreniak, Y. Guyot, R. Pazzik, W. Streck, C. Goutaudier, G. Boulon, *J. Phys.: Condens. Matter.* 19 (2006) 1.